Available online at www.sciencedirect.com
SCIENCE DIRECT®
Journal of Power Sources 142 (2005) 1–9
JOURNAL OF POWER SOURCES
www.elsevier.com/locate/jpowsour

Ionic and electron–hole conduction in $BaZr_{0.93}Y_{0.07}O_{3-\delta}$ by 4-probe dc measurements

Wensheng Wang, Anil V. Virkar*

Department of Materials Science and Engineering, 122S Central Campus Drive, University of Utah, Salt Lake City, UT 84112, USA

Received 20 August 2004; accepted 12 September 2004
Available online 2 December 2004

Abstract

Porous samples of composition of $BaZr_{0.93}Y_{0.07}O_{3-\delta}$ were fabricated. Electrical conductivity of porous samples was measured using a 4-probe dc method over a p_{O_2} range from 7.3×10^{-6} to 1 atm and over a temperature range from 500 to 800 °C. The results showed that the electrical conductivity increases with increasing p_{O_2}, a characteristic of electron–hole conduction. Above p_{O_2} of 0.01 atm, the measured total conductivity was fitted to $\sigma_t = \sigma_i + fp_{O_2}^{1/4}$, where σ_i is the ionic conductivity and $fp_{O_2}^{1/4}$ is the electronic (hole) conductivity. The activation energies were estimated to be $\sim 0.57 \pm 0.15$ and $\sim 1.01 \pm 0.04$ eV for oxygen ion and electron–hole conduction, respectively. The oxygen ion transference number ranged between ~0.01 and 0.7 over the p_{O_2} and the temperature ranges investigated. Electrical conductivity measurements were also carried out in H_2O-containing atmospheres. It was observed that at a temperature below ~550 °C, the predominant ionic conduction was due to protons.

Keywords: Barium zirconate; Perovskite; Oxygen ion conduction; Electron–hole conduction; Proton conduction

1. Introduction

Many perovskite oxides, such as rare earth oxide doped $BaCeO_3$, $SrCeO_3$, $BaZrO_3$, to name a few, and off-stoichiometric mixed perovskites such as $Ba_3Ca_{1.18}Nb_{1.82}O_{9-\delta}$ (BCN18), exhibit proton conduction when exposed to a humid atmosphere at elevated temperatures [1–6]. This property makes them promising candidates for a variety of applications, such as solid oxide fuel cells (SOFCs), gas sensors, H_2 separation or purification membranes, hydrogenation/dehydrogenation of hydrocarbons, etc. [7–9]. Of these materials, the cerate-based oxides and BCN18 have been shown to exhibit some of the highest proton conductivities [10]. For example, the proton conductivity of some of the cerate-based materials is greater than the oxygen ion conductivity of 8 mol.% yttria-stabilized zirconia (8YSZ) at ~650 °C [11]. The cerates, however, are known to be unstable in humid or CO_2-containing atmospheres at temperatures below 500 °C, a property which makes their application in SOFCs difficult [12–16].[1] Zirconates, on the other hand, are stable in H_2O and CO_2-containing atmospheres [19]. Of the zirconates investigated so far, Y-doped $BaZrO_3$ has been reported to exhibit high proton conductivity and good chemical stability [20,21].

Several groups have investigated electrical conduction in Y-doped $BaZrO_3$ [11–16,19–25]. The reported electrical conductivity values, however, vary over a wide range. For example, the reported interior (bulk) electrical conductivity of $BaZr_{0.9}Y_{0.1}O_{2.95}$ at 500 °C ranges between $\sim 10^{-7}$ [22] and $\sim 10^{-2}$ S cm^{-1} [21]. Electrical conductivity is often measured using ac impedance spectroscopy, especially when the objective is to separate the grain interior and grain boundary conductivities. Unambiguous resolution of grain boundary

* Corresponding author. Tel.: +1 801 581 5396; fax: +1 801 581 4816.
E-mail address: anil.virkar@m.cc.utah.edu (A.V. Virkar).

[1] It is to be noted, however, that fuel cells made using doped $BaCeO_3$ electrolytes (in dense form) have been operated for several days at elevated temperatures (typically >700 °C) [17,18].

0378-7753/$ – see front matter © 2004 Elsevier B.V. All rights reserved.
doi:10.1016/j.jpowsour.2004.09.031

impedance from bulk impedance, however, is often difficult due to overlapping spectra. Also, interpretation of ac impedance spectra is not straightforward and must be based on idealized microstructure models, equivalent circuit models and special data fitting techniques are often required. 4-Probe dc method, on the other hand, gives an unequivocal measure of the total conductivity. Contributions due to grain interior and grain boundary, however, cannot be readily determined by this method, unless measurements are made on samples of several grain sizes, such has been done for rare earth oxide doped ceria [26]. Still, from a practical standpoint, a 4-probe dc measurement is the desired one since in most devices, often it is the dc conductivity which is of interest.

It had been generally believed that Y-doped $BaZrO_3$ is a predominantly proton conductor in humid atmospheres. Recent work, however, suggests that significant electron–hole conduction is present in both dry and wet atmospheres at temperatures above 400 °C [23–25]. Ionic transference number has been measured using concentration cells [24,25]. This technique, however, gives an average value over the p_{O_2} gradient imposed. It has also been shown that partial conductivities due to oxygen ions, protons, electrons, and electron–holes can be estimated by electrical conductivity measurements in combination with a defect model by measuring the electrical conductivity at various p_{O_2}, p_{H_2O}, and temperatures [27–31]. In order to study the p_{O_2}- and the p_{H_2O}-dependence of electrical conductivity accurately, complete thermodynamic equilibrium between the gas phase and the solid phase is necessary. Dense samples of thickness ∼1 mm are often used in many experiments. However, for a typical diffusion coefficient, $\tilde{D} \sim 10^{-8}\ \mathrm{cm^2\ s^{-1}}$, the characteristic diffusion time given by $\ell^2/\tilde{D}$, where ℓ is half the thickness, is of the order of $\sim 10^6$ s or several hundred hours. If the equilibration kinetics is governed by surface kinetics, the corresponding characteristic time is ℓ/k_{exc}, where k_{exc} is the surface exchange coefficient with units of $\mathrm{cm\ s^{-1}}$, and is often of the order of $10^{-5}\ \mathrm{cm\ s^{-1}}$. This implies that upon a change of atmosphere, long equilibration times are necessary, which is impractical in typical experimental procedures employed, especially at low temperatures. Use of porous samples of appropriate microstructures has been shown to be an effective method of overcoming such difficulties [32,33]. The principle is that in a porous solid, the effective solid-state diffusion distance is of the order of the particle size, d, which is typically very small (a few microns) such that the characteristic time for equilibration is $d^2/\tilde{D}$, assuming that the surface reaction is rapid. If the kinetics is governed by the surface reaction, then the characteristic time is given by d/k_{exc}. Since the particle size in a porous sample is much smaller than the typical thickness of a dense sample, that is, since $d \ll \ell$, it is expected that equilibration time will be much smaller in porous samples. This assumes that gas transport into the porous interstices is rapid. If the pore size is large enough such that gas transport predominantly occurs by effective binary diffusion, the characteristic time required for equilibration of the atmosphere within the porous sample of thickness 2ℓ is of the order of ℓ^2/D_{eff}, where D_{eff} is the effective gas diffusion coefficient in a porous body, which is typically $>10^{-2}\ \mathrm{cm^2\ s^{-1}}$, and is generally of the order of $0.1\ \mathrm{cm^2\ s^{-1}}$. That is, for a sufficiently porous and thin sample, it can be assumed that gas composition rapidly equilibrates within the porous interstices. Thus, the kinetics of equilibration of the sample is dictated by solid-state diffusion into the particles. Therefore, the kinetics of equilibration is expected to be much faster in porous bodies as compared to dense samples. For this reason, in the present work, porous samples of Y-doped $BaZrO_3$ were used.

2. Theoretical basis

For a high temperature proton conductor, the relevant defect reactions may be written as

$$H_2O_{(gas)} + V_O^{\bullet\bullet} \Leftrightarrow O_O^{\times} + 2H^{\bullet}$$

with the equilibrium constant given by

$$K_W = \frac{[O_O^{\times}][H^{\bullet}]^2}{p_{H_2O}[V_O^{\bullet\bullet}]} \tag{1}$$

for H_2O incorporation, and

$$\tfrac{1}{2}O_{2(gas)} + V_O^{\bullet\bullet} \Leftrightarrow O_O^{\times} + 2h^{\bullet}$$

with the equilibrium constant given by

$$K_h = \frac{[O_O^{\times}]p^2}{p_{O_2}^{1/2}[V_O^{\bullet\bullet}]} \tag{2}$$

for oxygen incorporation, assuming that the law of mass action holds and that oxygen vacancies are fully ionized. The concentrations of the relevant charged species are governed by the electroneutrality condition, which is given by[2]

$$2[V_O^{\bullet\bullet}] + H^{\bullet} + p = [Y'] \tag{3}$$

Based on these equations and the Nernst relation, one can obtain the partial electrical conductivities due to the three carriers, which are functions of p_{H_2O}, p_{O_2}, K_W, K_h, and $[Y']$ (dopant content). If the predominant electronic conduction is by electron–holes, the total electrical conductivity can be usually described by

$$\sigma_t = \sigma_{ion} + f p_{O_2}^{1/n} \tag{4}$$

where σ_{ion}, the total ionic conductivity, is the sum of oxygen ion and proton conductivities, f the pre-exponential factor with dimensions of conductivity, and n is typically 4 or 6, depending on the p_{O_2} and the temperature regime. In a dry atmosphere, a plot of σ_t versus $p_{O_2}^{1/n}$ is expected to yield the partial conductivities due to oxygen ions and electron–holes.

[2] Here, only the high p_{O_2} regime is considered, such that electron concentration can be ignored. If the p_{O_2} is low such that electron concentration cannot be ignored, it will have to be included in the electroneutrality condition.

In H_2O-containing atmospheres, such a plot allows one to determine the proton conductivity.

3. Experimental procedure

3.1. Materials synthesis, characterization, and sample preparation

Powder of composition $BaZr_{0.93}Y_{0.07}O_{3-\delta}$ was synthesized by calcining a powder mixture of $BaCO_3$, ZrO_2, and Y_2O_3 at 1400 °C for 4 h. The calcined powder was mixed with fine carbon powder of particle size 10–20 μm and ball-milled, and bars were die-pressed, isostatically pressed under a pressure of ∼2000 kg cm^{-2}, followed by sintering in air at 1650 °C for 10 h.

The as-sintered sample was characterized by X-ray diffraction (XRD) with Cu Kα radiation. The microstructure of the fractured surface of a sintered sample was characterized using scanning electron microscopy (SEM). The apparent density of the sintered sample (porous) was measured using the Archimedes method [34].

Platinum paste was painted on porous samples to form four contacts in the form of strips. Four platinum wires were attached to each sample to form four leads for 4-probe dc measurements.

3.2. Conductivity measurement

The conductivity was measured using a 4-probe dc method described in detail elsewhere [32].

Initially, the sample was heated to ∼900 °C in dry air and the sample was maintained at temperature for over 5 h to minimize the background H_2O content in the sample. Then the sample was heated to the desired temperature in flowing dry air. Once the temperature stabilized, the conductivity was continuously monitored for a time long enough to ensure that a stable value was attained. The atmosphere in the chamber was then changed to a different p_{O_2}, and the procedure was repeated.

In order to investigate the effect of partial pressure of water vapor, the desired p_{H_2O} was obtained by passing a carrier gas (dry air or dry N_2) through a water bubbler maintained at the appropriate temperature.

4. Results

Fig. 1 shows an X-ray diffraction (XRD) pattern of an as-sintered $BaZr_{0.93}Y_{0.07}O_{3-\delta}$ sample, which corresponds to a simple cubic structure. The lattice constant determined from the peak at $2\theta = 30°$ is $a = 4.1914$ Å. For the composition $BaZr_{0.93}Y_{0.07}O_{2.965}$, the theoretical density is calculated to be 6.222 g cm^{-3}. The apparent density of the porous sample was measured to be 3.593 g cm^{-3}. Accordingly, the porosity of the sample is ∼42.3 vol.%.

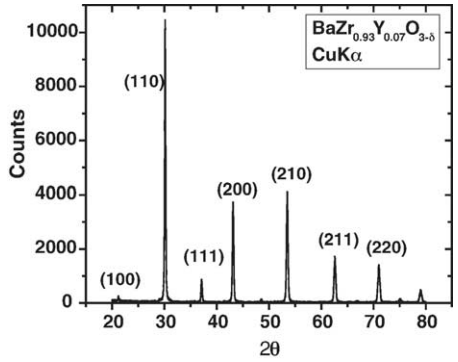

Fig. 1. X-ray diffraction pattern of an as-sintered $BaZr_{0.93}Y_{0.07}O_{3-\delta}$ sample.

Fig. 2 is an SEM micrograph of the fracture surface of a typical porous sample used in this work. The *Inset* is a micrograph at a higher magnification. The typical particle and pore sizes are of the order of a few microns.

Fig. 3 shows the time dependence of the normalized electrical conductivity, defined as

$$X(t) = \left| \frac{\sigma(t) - \sigma(0)}{\sigma(\infty) - \sigma(0)} \right| \quad (5)$$

where $\sigma(0)$, $\sigma(t)$ and $\sigma(\infty)$ are, respectively, the initial conductivity, the conductivity at time 't' after the change to a new atmosphere, and the conductivity after equilibration at the new atmosphere, during H_2O incorporation and O_2 desorption by a porous $BaZr_{0.93}Y_{0.07}O_{3-\delta}$ sample. It is seen that at 500 °C, it takes, respectively, 3 and 40 min for the porous material to attain equilibrium with new p_{H_2O} and new p_{O_2}.

The conductivity[3] was measured on a porous sample of nominal dimensions 2.36 mm × 10.64 mm × 47 mm as a function of p_{O_2} at several temperatures. First, the sample was exposed to pure oxygen ($p_{O_2} = 1$ atm) at 800 °C for a sufficiently long time to ensure that the conductivity attains a stable value. The stable value was recorded as that corresponding to the equilibrium conditions. With the temperature fixed at 800 °C, the same procedure was repeated in O_2–N_2 gas mixtures at subsequently lower values of p_{O_2}, specifically, 2.1×10^{-1}, 5×10^{-2}, 1×10^{-2}, 2×10^{-3}, 1×10^{-3}, 5×10^{-5}, and 7.3×10^{-6} atm. Subsequently, the temperature was decreased to 700, 600, 550, and 500 °C and at each temperature, the conductivity corresponding to equilibrium conditions was measured at each of the p_{O_2} levels stated above. The collected data at each temperature are plotted as a function of p_{O_2} on a log–log scale in Fig. 4(a). It is seen that $\log(\sigma)$ increases with increasing $\log(p_{O_2})$ and the dependence is linear for $p_{O_2} > 0.01$ with slopes close to 1/4. The data for $p_{O_2} > 0.01$ were then fitted to $\sigma_t = \sigma_O + f p_{O_2}^{1/4}$, and σ_t is

[3] In the following, conductivity means total conductivity.

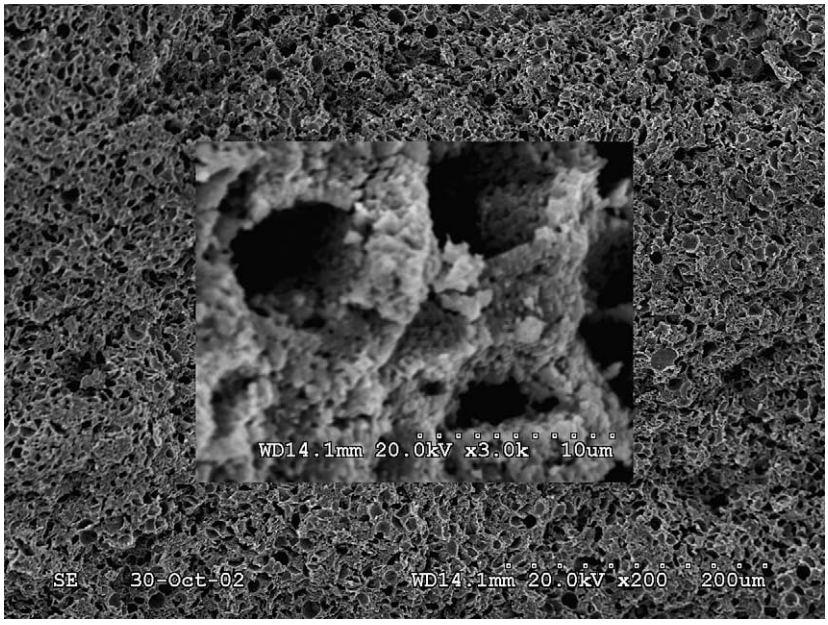

Fig. 2. An SEM micrograph of the fractured surface of a porous $BaZr_{0.93}Y_{0.07}O_{3-\delta}$ sample.

plotted versus $p_{O_2}^{1/4}$ in Fig. 4(b). Fitting result in values of σ_O as 2.06×10^{-5}, 2.07×10^{-5}, 2.03×10^{-5}, 4.12×10^{-5}, and 1.79×10^{-4}, and values for f as 9.15×10^{-5}, 3.42×10^{-4}, 6.95×10^{-4}, 2.56×10^{-3}, and 5.79×10^{-3} corresponding, respectively, to 500, 550, 600, 700, and 800 °C. $\log(T\sigma_O)$ and $\log(Tf)$ are plotted versus $1/T$ in Fig. 5. Assuming the electrical conductivities can be described by

$$\sigma = \frac{A}{T} \exp\left(-\frac{E_a}{T}\right),$$

where A is a pre-exponential factor independent of temperature T, the data were fitted to straight lines (Arrhenius fit). The activation energy, E_a, and pre-exponential factor, A, were then extracted from the plots, namely, $E_a = 0.57 \pm 0.15$ eV and $A = 55$ for oxygen ion conduction, and $E_a = 1.01 \pm 0.04$ eV and $A = 782305$ for electron–hole conduction, respectively.

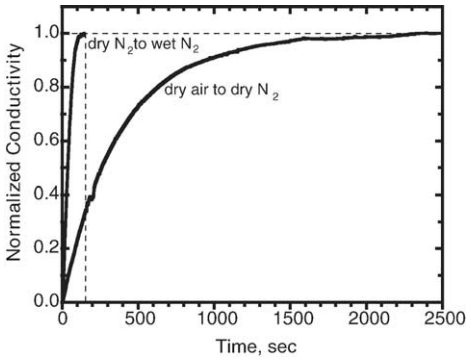

Fig. 3. Electrical conductivity relaxation during H_2O incorporation and O_2 desorption by a porous $BaZr_{0.93}Y_{0.07}O_{3-\delta}$ sample.

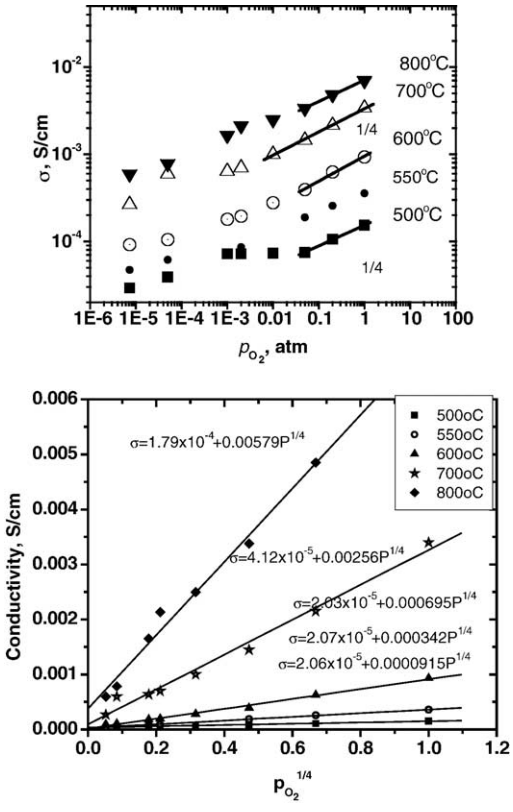

Fig. 4. (a) Total conductivity as a function of p_{O_2} (on a log–log scale) at five different temperatures measured in H_2O-free atmospheres and (b) total conductivity as a function of $p_{O_2}^{1/4}$ at five different temperatures measured in H_2O-free atmospheres.

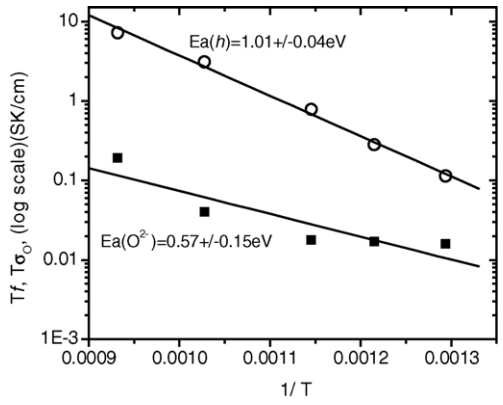

Fig. 5. $\log(T\sigma_O)$ and $\log(Tf)$ vs. $1/T$ for the estimation of activation energies for oxygen ion conduction and electron–hole conduction. The resultant expressions are $\sigma_O = \frac{55}{T}\exp\left(-\frac{6612}{T}\right)$ and $f = \frac{782305}{T}\exp\left(-\frac{11715}{T}\right)$.

Accordingly, the expressions obtained are

$$\sigma_O = \frac{55}{T}\exp\left(-\frac{6612}{T}\right)$$

and $$f = \frac{782305}{T}\exp\left(-\frac{11715}{T}\right).$$

The oxygen ion transference number, $t_O = \sigma_O/\sigma_t$, was calculated based on the σ_O obtained above, and the results at 500 and 700 °C are plotted as a function of p_{O_2} in Fig. 6. Over the p_{O_2} range from 7.3×10^{-6} to 1 atm, oxygen ion transference number decreases from ~0.7 to ~0.1 at 500 °C and from ~0.2 to ~0.01 at 700 °C.

In Fig. 7, $\log(T\sigma)$ is plotted versus $1/T$ for $p_{O_2} = 7.3 \times 10^{-6}$ and 1 atm, respectively. Fitting to straight lines yields two activation energies, specifically 0.81 and 1.01 eV, corresponding to $p_{O_2} = 7.3 \times 10^{-6}$ and 1 atm, respectively.

The conductivity was also measured at various p_{H_2O} and at 500 and 700 °C. Figs. 8 and 9 show the time-dependent (total) conductivity at 500 and 700 °C over a p_{H_2O} range from 0.006 to 0.47 atm. The sample was initially exposed to dry air with the corresponding stable value of conductivity being $\sim 9 \times 10^{-5}$ S cm^{-1} at 500 °C. The atmosphere was then abruptly changed from dry air to humid air with $p_{H_2O} = 0.006$ atm. When the conductivity reading became stable, the atmosphere was changed from humid air back to dry air. Similar dry–wet–dry cycles were repeated at

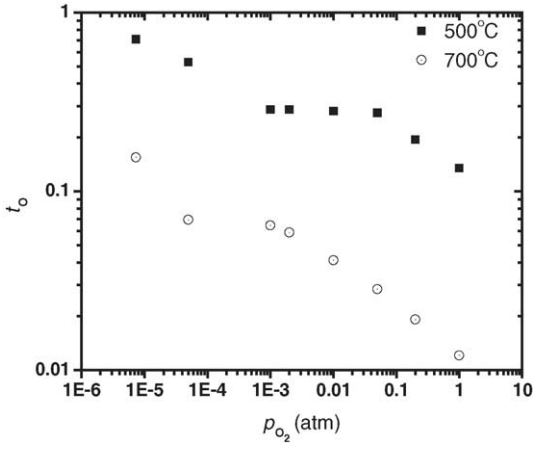

Fig. 6. Oxygen ion transference number vs. p_{O_2}. (■) 500 °C and (○) 700 °C.

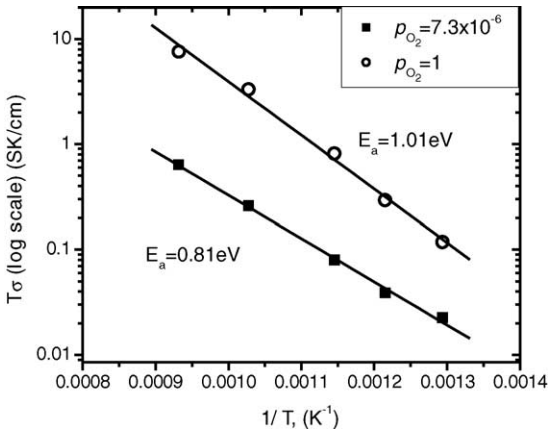

Fig. 7. $\log(T\sigma)$ vs. $1/T$. (■) $p_{O_2} = 7.3 \times 10^{-6}$ atm and (○) $p_{O_2} = 1$ atm.

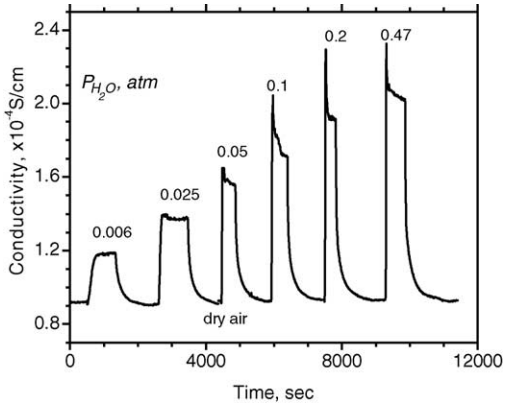

Fig. 8. Total conductivity vs. time for dry–wet–dry cycles corresponding to various p_{H_2O} at 500 °C.

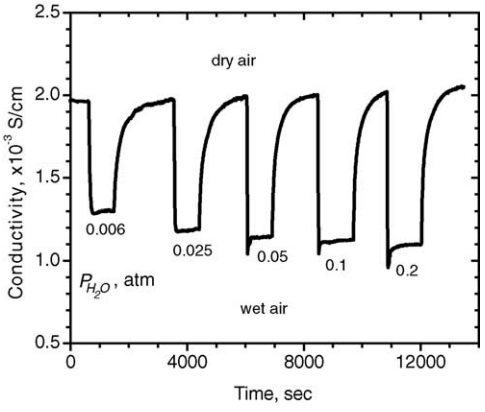

Fig. 9. Total conductivity vs. time for dry–wet–dry cycles corresponding to various p_{H_2O} at 700 °C.

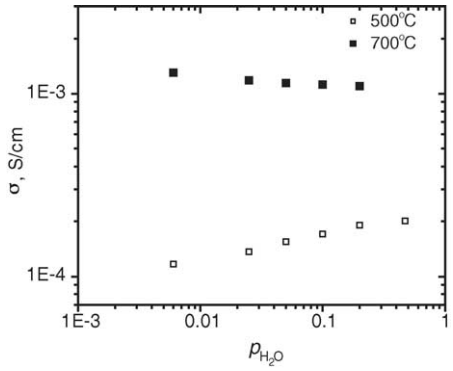

Fig. 10. Total conductivity vs. p_{H_2O}. (□) 500 °C and (■) 700 °C.

subsequently increasing p_{H_2O}. Fig. 8 shows that the conductivity increases with increasing p_{H_2O} at 500 °C. Similar experiments were carried out at 700 °C (Fig. 9), where in dry air, the corresponding conductivity was $\sim 2 \times 10^{-3}$ S cm^{-1}. As seen in Fig. 9, the conductivity decreases with increasing p_{H_2O} at 700 °C. Stable values of conductivity are plotted versus p_{H_2O} in Fig. 10 for both temperatures. The data were fitted to empirical expressions $(\sigma_{wet} - \sigma_{dry}) = 0.002 p_{H_2O}^{0.4}$ and $(\sigma_{wet} - \sigma_{dry}) = -0.00094 p_{H_2O}^{0.05}$ at 500 and 700 °C, respectively.

Conductivity was measured over a temperature range from 400 to 800 °C in dry air and wet air ($p_{H_2O} \sim 0.025$ atm), respectively. The results are plotted in Fig. 11. It is seen that the data for wet and dry air crossover at ∼550 °C; above 550 °C, the conductivity in dry air is larger, while, below ∼550 °C, the conductivity in wet air is larger. Also shown in the figure are data from Katahira et al. [25].

Conductivity was also measured in dry N_2 ($p_{O_2} \sim 0.001$ atm) and wet N_2 (p_{H_2O} 0.025 atm), respectively, over a temperature range from 500 to 800 °C; and the corresponding data are also shown in Fig. 11. It is seen that the conductivity in wet N_2 is higher than that in dry N_2 over the whole temperature range.

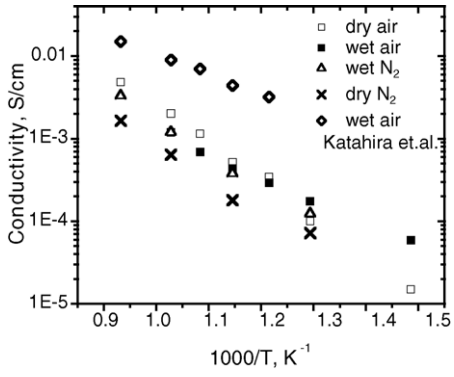

Fig. 11. Total conductivity (log scale) vs. 1/T. (□) Dry air, $p_{O_2} = 0.21$ atm; (■) wet air, $p_{H_2O} = 0.025$ atm; (△) wet N_2, $p_{O_2} = 0.001$ atm, $p_{H_2O} = 0.025$ atm; (×) dry N_2, $p_{O_2} = 0.001$ atm and (◊) data of Katahira et al. on a dense material, wet air, $p_{H_2O} = 0.017$ atm [25].

5. Discussion

5.1. Porous material versus dense material

Our previous work has demonstrated that porous samples of $Ba_3Ca_{1.18}Nb_{1.82}O_{9-\delta}$ (BCN18) exhibit similar dependency of electrical conductivity on p_{O_2}, p_{H_2O}, and temperature, as do dense samples, and magnitudes are also essentially the same when corrected for porosity [33]. In BCN18 samples used in the earlier work, the typical particle and pore sizes were of the order of a few microns. As such, the total number of surface atoms, relative to those in the bulk, was negligible. For this reason, the main differences between the conductivities of porous samples and dense samples are related to geometry; i.e., the pore volume fraction and particle morphology. Thus, apart from a geometric correction factor, the measurement of conductivity of porous bodies yields the same basic information as does the measurement on dense bodies. The same behavior is expected for porous $BaZr_{0.93}Y_{0.07}O_{3-\delta}$ samples used in this study. That is, the surface area introduced by porosity should have negligible effect on the properties of the porous material, as influenced for example, by adsorption of O_2 or H_2O. Based on the microstructure shown in Fig. 2, the maximum possible amount of H_2O adsorbed on surface is estimated to be less than 3% of the amount of H_2O dissolved in the bulk at a p_{H_2O} 0.025 atm and $T = 700$ °C. Thus, the effect of possible adsorbed species on the surfaces of pores can be ignored, and the measurement of conductivity of porous bodies yields essentially the same information as the measurement on dense bodies—apart from a geometric factor. The use of porous bodies, on the other hand, has important implications from the standpoint of the kinetics of equilibration—and thereby the establishment of equilibrium conditions in a reasonable period of time.

Fig. 3, for example, shows that in the porous $BaZr_{0.93}Y_{0.07}O_{3-\delta}$ sample at 500°C, H_2O incorporation required ∼3 min to attain equilibrium, while O_2 desorption required ∼40 min. The typical particle and pore sizes are of the order of a few microns (∼10 μm). Gas transport in and out of the porous interstices can be shown to be very fast, as the effective O_2–N_2 diffusion coefficient for gaseous transport through porous bodies with porosity ∼30–40% is typically of the order of ∼0.1 cm^2 s^{-1}. By contrast, solid-state transport into the particles is expected to be much slower. Thus, assuming transport by diffusion[4] into the particles of the material is the rate-limiting step, the time required for this step is approximately proportional to $x^2/\tilde{D}$, where x is the smallest dimension of the sample, and $\tilde{D}$ refers to the chemical diffusion coefficient of the diffusing species in the material (here either of O_2 (or O) or H_2O, depending upon the atmosphere). For a dense $BaZr_{0.93}Y_{0.07}O_{3-\delta}$ sample of 1 mm (1000 μm) thickness, the time required to attain equilibrium would be (1000 μm/10 μm) = 10^4 times larger than

[4] If surface exchange is the limiting step, the time required will be proportional to x/k_{exc}.

the time required by the porous sample used in this study, that is, ∼8 h for H_2O incorporation or ∼111 h for O_2 desorption. Clearly, the attainment of equilibrium conditions in a reasonable time, when using a dense sample of ∼1 mm thickness, is not expected. For this reason, porous samples were used in the present work. Faster kinetics of H_2O uptake (∼3 min) compared to relatively slow O_2 desorption (∼40 min) suggests that $\tilde{D}_{H_2O}$ must be greater than $\tilde{D}_O$.

5.2. Conductivity in a dry atmosphere

5.2.1. p_{O_2} Dependence

Fig. 4(a) shows that the conductivity increases with increasing p_{O_2} at each of the temperatures examined, a characteristic of electron–hole conduction. For $p_{O_2} > 0.01$ atm, the conductivity can be satisfactorily described by $\sigma_t = \sigma_O + fp_{O_2}^{1/4}$ (Fig. 4(b)). For $p_{O_2} \leq 0.01$ atm, the p_{O_2}-dependence of conductivity exhibits smaller slopes. These findings are consistent with the observations by others [23,24] on dense samples of $BaZr_{0.9}Y_{0.1}O_{3-\delta}$ over a similar temperature range.

5.2.2. Oxygen ion transference number

Ionic transference number is a measure of the relative contribution of ionic conduction to the total electrical conduction. It is observed in Fig. 6 that the oxygen ion transference number, t_O, depends not only on temperature but also on p_{O_2} in such a way that t_O decreases with increasing T and increasing p_{O_2}. The p_{O_2}-dependence is readily understandable from reaction (2), while, the T-dependence of t_O is attributed to the endothermic nature of the oxygen incorporation reaction (Eq. (2)). For materials such as Y-doped $BaZrO_3$, the oxygen vacancy concentration is dominated by the dopant level ([Y′]), and the electron–hole concentration is dominated by reaction (2). In this situation, the oxygen vacancy concentration is approximately independent of temperature and p_{O_2} over a wide range, while the electron–hole concentration increases with increasing temperature.

5.2.3. Temperature dependence

The electrical conductivity due to an ionic charge carrier is usually described by

$$\sigma = \frac{A}{T}\exp\left(-\frac{E_a}{T}\right),$$

where A, the pre-exponential factor, is a function of concentration and vibrational frequency of the charge carrier. In many oxides, the motion of electron–holes occurs by hopping and is thermally activated, unlike the motion of free electrons or electron–holes in semiconductors. Therefore, the preceding expression also applies to electron–hole conductivity. In the previous section, activation energy of $\sim 0.57 \pm 0.15$ eV was determined for oxygen ion conduction, which is much lower than the value $\sim 1.1 \pm 0.1$ eV measured for the grain interior of dense $BaZr_{0.9}Y_{0.1}O_{3-\delta}$ by Bohn et al. [23]. Such a difference is not surprising in that the value in reference [23] was obtained over a lower temperature range and using ac impedance spectroscopy. It is to be noted that activation energy values of 0.46 and 0.54 eV were obtained for, respectively, $BaThO_3$ [29] and BCN18 [33], which are of the same order of magnitude as in the present work. For electron–hole conduction, activation energy of $\sim 1.01 \pm 0.04$ eV was obtained in this study (Fig. 5), which consists of two contributions, specifically, the activation energy associated with the motion of electron–holes and the enthalpy for the formation of one electron–hole from oxygen incorporation reaction as shown by Eq. (2). Usually the activation energy for electron–hole motion is of the order of ∼0.1 eV. Thus the enthalpy for reaction (2) is estimated to be of the order of ∼1.8 eV. In Fig. 7, the slope of $\log(T\sigma)$ versus $1/T$ exhibits dependence upon p_{O_2}. At $p_{O_2} = 1$ atm, when the electrical conduction is dominated by electron–hole conduction ($t_h > 0.9$), an activation energy of 1.01 eV is obtained, which is consistent with the result shown in Fig. 5. At $p_{O_2} = 7.3 \times 10^{-6}$ atm, by contrast, a smaller slope is observed, resulting in a lower activation energy of ∼0.81 eV. At this p_{O_2}, the t_O varies from 0.1 to 0.7 depending on temperature, indicating that electrical conduction changes from predominantly electron–hole conduction to predominantly oxygen ion conduction with decrease in p_{O_2} from 1 atm to 7.3×10^{-6} atm. Presumably, at a sufficiently low p_{O_2}, oxygen ion conduction is substantial over the temperature range, and the slope of $\log(T\sigma)$ versus $1/T$ should be closer to the activation energy for oxygen ion conduction. The observation that the estimated activation energy corresponding to $p_{O_2} = 7.3 \times 10^{-6}$ atm is 0.81 eV is consistent with this expectation. That is, at a p_{O_2} of 7.3×10^{-6} atm, there is a significant contribution from both electron–holes and oxygen ions to total conduction over the temperature range studied. Therefore, the value 0.57 ± 0.15 eV for oxygen ion transport appears to be reasonable.

From the obtained values for E_a and A, the total electrical conductivity in dry atmosphere may be described by

$$\sigma = \frac{55}{T}\exp\left(-\frac{6612}{T}\right) + \frac{782305}{T}\exp\left(-\frac{11715}{T}\right)p_{O_2}^{1/n} \quad (6)$$

where n depends on the p_{O_2} range, and is ∼4 for $p_{O_2} > 0.01$ atm. For a dense material, a correction for porosity must be made to the above expression.

5.3. Conductivity in wet atmosphere

When a proton conductor is exposed to a humid atmosphere, H_2O is incorporated into the material to fill up oxygen vacancies, and as a result, the concentrations of oxygen vacancies and electron–holes decrease and that of protons increases. Concurrently, proton conductivity increases at the expense of oxygen ion and electron–hole conductivities. The total conductivity, however, can either increase or decrease, depending on the magnitudes of the governing parameters for the conductivities due to each type of charge carrier. For BCN18, a mixed oxygen ion and electron–hole conductor in

dry air, the total conductivity increases with the absorption of H_2O at temperatures up to 800 °C [32]. Unlike BCN18, the total conductivity of $BaZr_{0.93}Y_{0.07}O_{3-\delta}$ decreases with increasing p_{H_2O} above 550 °C, and increases with increasing p_{H_2O} below 550 °C. Similar behavior was observed in $BaThO_3$ [29,30]. Such a behavior can be generally attributed to the fact that electron–hole conductivity exhibits stronger dependence on temperature and p_{O_2} compared to proton conductivity. Consequently, the increase in proton conductivity is less than the decrease in electron–hole conductivity at elevated temperatures or high p_{O_2} while the increase in proton conductivity exceeds the decrease in electron–hole conductivity at lower temperatures or lower p_{O_2}. It is seen from Fig. 11 that the electrical conductivity in wet air exceeds that in dry air at $T \leq 550$ °C, which almost doubles at 500 °C, and is about four times at 400 °C. This indicates that proton conduction predominates, i.e., $t_H > 0.5$, in wet air at temperatures below 500 °C. Under similar conditions, by contrast, t_H of less than 0.03 was obtained using concentration cells [24]. The origin for the discrepancy is unclear. It is possible that equilibrium conditions were not achieved when dense samples were used, such as in the work reported in [24].

For the purposes of comparison, the total conductivities of dense $BaZr_{0.9}Y_{0.1}O_{3-\delta}$ reported by Katahira et al. [25] are plotted in Fig. 11. It is seen that the data in wet air obtained in this work are smaller by a factor of ~10 for all the temperatures compared. Taking into account the factors of porosity and differences in dopant levels, the present result is qualitatively comparable to those by Katahira et al. [25]. This agreement further demonstrates that porous and dense samples of $BaZr_{0.93}Y_{0.07}O_{3-\delta}$ exhibit similar dependency of electrical conductivity on p_{O_2}, p_{H_2O} and temperature, corrected for porosity. As the kinetics of equilibration are considerably more rapid in porous samples, it is expected that the results obtained in the present work are closer to equilibrium values than those obtained on dense samples, especially at lower temperatures.

6. Summary

Porous $BaZr_{0.93}Y_{0.07}O_{3-\delta}$ samples with ~42.3 vol.% porosity were fabricated and the electrical conductivity was investigated using a 4-probe dc method as a function of p_{O_2}, p_{H_2O}, and temperature. Use of porous materials facilitates rapid equilibration with the gas phase, e.g., with oxygen and H_2O. Timed data acquisition ensured the measurement of electrical conductivities corresponding to equilibrium conditions at various oxygen and H_2O partial pressures. Based on prior work on porous and dense BCN18, it is expected that results on porous $BaZr_{0.93}Y_{0.07}O_{3-\delta}$ corrected for porosity should exhibit similar dependency of electrical conductivity on p_{O_2}, p_{H_2O}, and temperature as the dense samples. Measurements corresponding to equilibrium conditions, however, are generally not possible due to slow kinetics, especially at low temperatures. Partial electrical conductivities due to oxygen ions and electron–holes were determined over the temperature range from 500 to 800 °C. The activation energies were determined to be $\sim 0.57 \pm 0.15$ and $\sim 1.01 \pm 0.04$ eV for oxygen ion and electron–hole conduction, respectively. Also, the oxygen ion transference number ranged between ~0.01 at $p_{O_2} = 1$ atm and 700 °C to ~0.7 at $p_{O_2} = 7.3 \times 10^{-6}$ atm and 500 °C. Electrical conductivity measurements were also carried out in H_2O-containing atmospheres, which showed predominantly proton conduction at temperatures below 500 °C. In addition, p_{O_2}- and p_{H_2O}-dependence of the electrical conductivity indicates that $BaZr_{0.93}Y_{0.07}O_{3-\delta}$ is a possible candidate as a conductimetric sensor for oxygen or humidity.

Acknowledgement

This work was supported by the U.S. Department of Energy, under Grant No. DE-FG02-03ER46086.

References

[1] H. Iwahara, Proton conduction in sintered oxides and its application to steam electrolysis for hydrogen production, Solid State Ionics 3–4 (1981) 359.
[2] H. Iwahara, H. Uchida, S. Tanaka, High-temperature type proton conductor based on strontium cerium trioxide and its application to solid electrolyte fuel cells, Solid State Ionics 9–10 (Pt. 2) (1983) 1021–1025.
[3] H. Iwahara, H. Uchida, K. Ono, K. Ogaki, Proton conduction in sintered oxides based on barium cerate ($BaCeO_3$), J. Electrochem. Soc. 135 (1988) 529.
[4] J.F. Liu, A.S. Nowick, The incorporation and migration of protons in neodymium-doped barium cerium oxide ($BaCeO_3$), Solid State Ionics 50 (1992) 131–138.
[5] T. Yajima, H. Suzuki, T. Yogo, H. Iwahara, Protonic conduction in strontium zirconate ($SrZrO_3$)-based oxides, Solid State Ionics 51 (1992) 101–107.
[6] K.C. Liang, Y. Du, A.S. Nowick, Fast high-temperature proton transport in nonstoichiometric mixed perovskites, Solid State Ionics 69 (1994) 117–120.
[7] Ph. Colomban (Ed.), Proton Conductors: Solids, Membranes and Gels-Materials and Devices, Cambridge University Press, Cambridge, 1992.
[8] H. Iwahara, Technological challenges in the application of proton conducting ceramics, Solid State Ionics 77 (1995) 289–298.
[9] T. Norby, Solid-state protonic conductors: principles, properties, progress and prospects, Solid State Ionics 125 (1999) 1–11.
[10] A.S. Nowick, Y. Du, High-temperature protonic conductors with perovskite-related structures, Solid State Ionics 77 (1995) 137.
[11] T. Hibino, A. Hashimoto, M. Suzuki, M. Sano, A solid oxide fuel cell using Y-doped $BaCeO_3$ with Pd-loaded FeO anode and $Ba_{0.5}Pr_{0.5}CoO_3$ cathode at low temperatures, J. Electrochem. Soc. 149 (11) (2002) A1503–A1508.
[12] M.J. Scholten, J. Schoonman, J.C. van Miltenburg, H.A.J. Oonk, Synthesis of strontium and barium cerate and their reaction with carbon dioxide, Solid State Ionics 61 (1993) 83.
[13] S. Goplan, A.V. Virkar, Thermodynamic stabilities of $SrCeO_3$ and $BaCeO_3$ using a molten salt method and galvanic cells, J. Electrochem. Soc. 140 (1994) 1060–1064.

[14] N. Taniguchi, T. Gamo, Structure changes of $BaCe_{0.8}Gd_{0.2}O_{3-\delta}$ electrolyte for fuel cell at high temperature in air and CO_2 atmosphere, Denki Kagaku oyobi Kogyo Butsuri Kagaku 62 (1994) 326.
[15] N. Bonanos, K.S. Knight, B. Ellis, Perovskite solid electrolytes: structure, transport properties and fuel cell applications, Solid State Ionics 79 (1995) 161.
[16] C.W. Tanner, A.V. Virkar, Instability of $BaCeO_3$ in H_2O-containing atmospheres, J. Electrochem. Soc. 143 (1996) 1386–1389.
[17] W.G. Coors, D. Zhong, Differential resistance analysis of protonic ceramic fuel cells for measuring bulk conductivity, Solid State Ionics 162–163 (2003) 283–290.
[18] W.G. Coors, Protonic ceramic fuel cells for high-efficiency operation with methane, J. Power Sources 118 (1–2) (2003) 150–156.
[19] H. Iwahara, T. Yajima, T. Hibino, K. Ozaki, Protonic conduction in calcium, strontium, and barium zirconates, Solid State Ionics 61 (1993) 65–69.
[20] K.D. Kreuer, Aspects on the formation and mobility of protonic charge carriers and the stability of perovskite-type oxides, Solid State Ionics 125 (1999) 285–302.
[21] K.D. Kreuer, Proton-conducting oxides, Annu. Rev. Mater. Res. 33 (2003) 333–359.
[22] R.C.T. Slade, S.D. Flint, N. Singh, Investigation of protonic conduction in Yb- and Y-doped barium zirconates, Solid State Ionics 82 (1995) 135–141.
[23] H.G. Bohn, T. Schober, Electrical conductivity of the high-temperature proton conductor $BaZr_{0.9}Y_{0.1}O_{2.95}$, J. Am. Ceram. Soc. 83 (4) (2000) 768–772.
[24] T. Schober, H.G. Bohn, Water vapor solubility and electrochemical characterization of the high temperature proton conductor $BaZr_{0.9}Y_{0.1}O_{2.95}$, Solid State Ionics 127 (2000) 351–360.
[25] K. Katahira, Y. Kohchi, T. Shimura, H. Iwahara, Protonic conduction in Zr-substituted $BaCeO_3$, Solid State Ionics 138 (2000) 91–98.
[26] S.J. Hong, K. Mehta, A.V. Virkar, Effect of microstructure and composition on ionic conductivity of rare-earth oxide-doped ceria, J. Electrochem. Soc. 145 (2) (1998) 638–647.
[27] G.-M. Choi, H.L. Tuller, Defect structure and electrical properties of single-crystal barium strontium titanate ($Ba_{0.03}Sr_{0.97}TiO_3$), J. Am. Ceram. Soc. 71 (4) (1988) 201–205.
[28] N. Bonanos, Transport study of the solid electrolyte barium cerium gadolinium oxide ($BaCe_{0.9}Gd_{0.1}O_{2.95}$) at high temperatures, J. Phys. Chem. Solids 54 (7) (1993) 867–870.
[29] T. Tsuji, T. Suzuki, H. Iwahara, Electrical conduction in $BaThO_3$ doped with Nd_2O_3, Solid State Ionics 70–71 (1994) 291.
[30] T. Tsuji, N. Miyajima, M. Ochida, Electrical conduction in $BaThO_3$ doped with Y_2O_3, Solid State Ionics 79 (1995) 183–187.
[31] H.-D. Baek, Modeling of electrical conductivity in high-temperature proton-conducting oxides, Solid State Ionics 110 (1998) 255–262.
[32] W. Wang, A.V. Virkar, A conductimetric humidity sensor based on proton conducting perovskite oxides, Sens. Actuators B 98 (2004) 282–290.
[33] W. Wang, A.V. Virkar, Determination of ionic and electronic conductivities of $Ba_3Ca_{1.18}Nb_{1.82}O_{9-\delta}$ (BCN18) in dry and wet atmospheres, J. Electrochem. Soc. 151 (10) (2004) 1565–1571.
[34] ASTM Standards, Standard Test Methods for Apparent Porosity, Water Absorption, Apparent Specific Gravity, and Bulk Density of Burned Refractory Brick and Shapes by Boiling Water, June 2000.